Korean J. Chem. Eng., 37(1), 54-64 (2020)
DOI: 10.1007/s11814-019-0428-2

pISSN: 0256-1115
eISSN: 1975-7220

Catalytic oxidation of benzene over alumina-supported Cu-Mn-Ce mixed oxide catalysts

Yang Gao, Jun Xiao†, Jiandong Ye, Xiaodong Huo, and Yutong Shen

Key Laboratory of Energy Thermal Conversion and Control of Ministry of Education, School of Energy and Environment, Southeast University, Nanjing, China
(*Received 17 July 2019 • accepted 12 November 2019*)

Abstract−Based on the response surface methodology (RSM), Cu-Mn-Ce catalysts were prepared via the vacuum impregnation method. Also, Their performance in the oxidation of a tar model compound (Benzene, 5,000 ppm) was evaluated. Results show that the optimum condition is CuO-MnO content of 30% and CeO_2 content of 4.4% at a calcination temperature of 620 °C for 4.1 h. In this condition, the confirmatory experiment indicates the average carbon conversion rate within half an hour ($X_{c\text{-}0.5h}$) and four hours ($X_{c\text{-}4h}$) are 99.5% and 97.1% at 300 °C, respectively, which is in good agreement with the model prediction. XRD, H_2-TPR, SEM, and XPS were employed in catalyst characterization. CuO is the primary active metal in the catalysts, which is affected easily by the calcination temperature. A lower calcination temperature tends to cause a weak structure strength, but a higher temperature results in impairing the reducibility. The major roles of CeO_2 are displayed in two aspects that CeO_2 increases the dispersion of the active metal, enhances the catalyst stability, and increases the oxygen vacancies and improves the oxygen transfer ability. For Cu-Mn-Ce composite catalyst, the catalytic oxidization of benzene complies with the Mars-van Krevelen mechanism (MVK). The content of CuO-MnO determines the number of active sites on the catalyst, which promotes the reduction of catalyst. CeO_2 plays an important role in enhancing the oxidization of the catalyst. Therefore, the ratio of CuO-MnO to CeO_2 in the catalyst will cause a change of the control step of the redox reaction.

Keywords: Benzene, Ceria, Copper Oxide, Redox Mechanism, Response Surface Methodology

INTRODUCTION

With the reduction of traditional fossil energy and the increasingly serious environmental problems, the utilization of renewable energy becomes more and more popular. Biomass is a promising renewable energy source due to its large reserves, low price and low pollution [1]. And biomass gasification can generate syngas of high calorific value, which is convenient for storage and transportation [2]. Therefore, biomass gasification has been receiving more and more attention [3,4]. However, hazardous tar produced in biomass gasification cannot be completely removed via the reforming process [5]. Therefore, how to eliminate biomass tar at lower temperatures is critical to biomass gasification.

Steam reforming is a conventional method for removing tar for biomass gasification [6,7]. However, tar is not easy to be converted entirely to small molecular gas, and the reforming reactions must occur at a higher temperature (>500 °C) [8]. From the previous reports, catalytic oxidation of volatile organic compounds with air can be carried out at lower temperatures (200 to 500 °C), saving energy and avoiding the formation of thermal NO_x [9,10]. Tar, being one of the organic compounds, the catalytic oxidation is an efficient, economic and environmentally technical mean for tar removal [11,12]. The main components in tar are benzene derivatives and polycyclic aromatic hydrocarbons. Hence, some researchers use benzene as the tar model compound [13,14].

Noble metal catalysts are commonly used in industry to catalyze the oxidation of benzene, such as supported Pd and Pt catalysts [15,16]. It is widely recognized that supported Pt catalysts are the most efficient catalysts for the oxidation of aromatic hydrocarbon oxidation [17-19], and the Au-Pd catalyst exhibits a higher activity due to its better reducibility [20]. Moreover, the noble metal catalysts show good resistance to water [21,22], but their applications are limited because of insufficient reserves and high costs [23,24]. Although some researchers adopt the single-atom method to reduce the consumption of noble metals in the preparation and utilization process of catalysts [25], this method is still in the laboratory research stage. Therefore, more researchers are paying attention to non-precious catalysts, such as manganese, nickel, copper, and iron [26-29]. Sang [28] reported that Cu/Al_2O_3 showed the best catalytic activity for the oxidation of toluene among Cu, Co, Ni, and Fe. Nevertheless, the different metals each have an advantage, and the synergistic effects between the metals are exhibited. Therefore, composite catalysts tend to have a better performance. Siham [30] reported that Cu/Mn could form a spinel structure oxide at a certain ratio and the activity of $Cu_{1.5}Mn_{1.5}O_4$ was better than CuO. Several studies showed that CuO-CeO_2 materials had high activity for a range of different oxidation reactions [17]. He [27] found that a large amount of Cu^{2+} in $CuCeO_x$ entered the CeO_2 lattice in the form of $Cu_xCe_{1-x}O_{2-\delta}$ solid solution, which generated a large number of oxygen holes on the surface of CuO_x and CeO_2 oxides improving the catalytic activity. Yang [31] found that when the content of Mn and Ce was 10% and the Mn/Ce molar ratio was

†To whom correspondence should be addressed.
E-mail: jxiao@seu.edu.cn

9, the catalyst could completely promote the oxidization of the low concentration benzene (1,000 ppm) at 260 °C. Lin [22] reported that Cu-Mn-Ce had higher activity for CO oxidation coupling Cu-Ce and Cu-Mn. The reason is due to the synergistic effects in the interfaces of Cu-Mn and Cu-Ce oxides [22,32-34]. The active metal Cu and Mn presented the oxidization ability, while Ce showed its high oxygen storage capacity and ability to enhance oxygen migration [35-37].

The mechanisms of catalytic oxidation of volatile organic compounds (VOC) have been systematically investigated [17]. Generally, Mars-van Krevelen (MVK), Langmuir-Hinshelwood (LH) and Eley-Rideal (ER) are used to explain the catalytic oxidization [38-41]. Among them, Mars-van Krevelen (MVK), which is called the redox mechanism, is accepted by most researchers, because the kinetic model corresponding to the MVK mechanism is highly consistent with the experimental data [38,40]. MVK mechanism is divided into two steps: (1) Reduction step: reduction of the oxidized catalyst by organic compounds; (2) Oxidation step: oxidation of the reduced catalyst sites by O_2. During the reaction, the catalyst is reduced and oxidized simultaneously, maintaining a cycle. However, the literature has not drawn a definite conclusion, which step is the control step of catalytic oxidation [37-40]. Li [37] found that the reduction step is higher than the oxidation step of benzene combustion over the $NiMnO_3/CeO_2$/Cordierite. On the other hand, Behar [42] got the opposite result in catalytic oxidation of toluene using $Cu_{1.5}Mn_{1.5}O_4$. The physicochemical properties of catalyst, reaction conditions and the pollutant composition will influence the reaction process. Therefore, it is important for the catalyst to consistently enhance the rates of two steps.

This study aim was to prepare the composite catalysts for catalytic oxidization of tar at a low temperature. Therefore, based on the response surface methodology (RSM), the preparation parameters of Cu-Mn-Ce catalysts were optimized. Benzene was used as a tar model compound to evaluate the catalyst performance. The control step in the catalytic oxidation reaction was also investigated in this study, based on the catalytic oxidation experiment of benzene and characterization of catalysts.

EXPERIMENT

1. Materials

All of the Cu-Mn-Ce supported catalysts in this experiment were

Table 1. Experimental design conditions and results

Case	CuO-MnO	CeO_2	Temperature	Calcination time	$X_{c\text{-}0.5h}$	$X_{c\text{-}4h}$
1	20	2.5	600	6	59.3	47.4
2	20	4.5	600	8	67.0	66.5
3	30	4.5	600	6	95.6	91.4
4	30	2.5	600	4	98.8	92.6
5	30	2.5	700	6	48.2	45.4
6	20	2.5	500	8	84.1	65.4
7	20	4.5	700	6	79.0	66.7
8	20	2.5	600	6	53.9	46.2
9	30	2.5	500	6	76.0	56.4
10	10	4.5	600	6	70.3	46.2
11	10	2.5	500	6	79.2	69.4
12	20	2.5	700	8	33.4	32.7
13	20	0.5	600	4	58.3	48.9
14	20	2.5	700	4	47.7	43.0
15	20	2.5	600	6	56.8	46.6
16	30	2.5	600	8	92.4	85.8
17	10	0.5	600	6	45.4	42.8
18	10	2.5	700	6	46.8	40.1
19	10	2.5	600	8	39.9	37.1
20	20	4.5	500	6	48.1	38.0
21	20	0.5	700	6	61.3	53.5
22	20	0.5	500	6	67.8	59.0
23	20	2.5	600	6	60.6	49.2
24	20	2.5	500	4	74.0	52.5
25	30	0.5	600	6	77.7	68.6
26	20	2.5	600	6	54.7	43.5
27	20	0.5	600	8	48.8	46.8
28	20	4.5	600	4	67.9	65.1
29	10	2.5	600	4	50.0	41.8

prepared using the vacuum impregnation method. First, Al_2O_3 carrier (Nanjing Aotai catalyst carrier Co. Ltd., China) was calcined at 600 °C for 4 h to prepare γ-Al_2O_3. According to a certain metal molar ratio, $Cu(NO_3)_2$, $Mn(NO_3)_2$ and $Ce(NO_3)_3$ were arranged in deionized water, and the active metals in the catalyst were represented by CuO, MnO, and CeO_2, respectively. The molar ratio of Cu/Mn is 3. The solute reagent details are shown in supporting information (not shown here, see Supplementary Data Table 1). The prepared solution was impregnated onto the γ-Al_2O_3 carrier under vacuum. It placed under vacuum for 20 h, dried at 105 °C for 24 h, and subsequently calcined in a muffle furnace to obtain the corresponding catalyst. After calcination, the catalyst was naturally cooled and sieved (0.3 to 0.6 mm).

The active metal content (wt%), calcination temperature (°C) and calcination time (h) of the catalysts were investigated in the experiment, and the catalysts were recorded as (CuO-MnO)-CeO_2-calcination temperature-calcination time.

Benzene is the representative of aromatic hydrocarbons. The previous study of our group [43] indicated that the content of benzene was maximum in residual substance after the tar reforming stage of biomass gasification. Therefore, benzene was selected as the tar model compound in the tar oxidation experiment.

2. Experimental System

The experiment was carried out in a fixed bed reactor. The schematic illustration of the experimental system is shown in the supporting information (not shown here; see the Supplementary Data Fig. 1). The benzene entered the feed pipe through a syringe pump at a flow rate of 1 ml/h. The temperature of the entire feed line was maintained at 150 °C. After the benzene vaporizing in the pipe, it was mixed with air (830 ml/min) in a cavity. In the mixed gas, the volume fraction of benzene was 5,000 ppm. The mixed gas was fed into a quartz reactor (the inner diameter is 25 mm and the height is 300 mm) to react. Before the reaction, 3.25 g of catalyst was placed on the stainless steel screen in the reactor, and the initial temperature of the reaction zone was maintained at 300 °C by the electric heating control system. After the reaction, the raw product gas was cooled by passing through the cooling device. After cooling, it was purified by passing the absorption device, where ethanol filter bottle combined with a bottle of allochroic silica gel was involved. Finally, the purified gas collection was carried out with a gas bag. The reaction kept 240 min, in which a bag of gas was collected every 5 min. Content analysis of collected gas compositions (CO_2, O_2, and N_2) was performed by GC (Agilent 6890N).

3. Experimental Scheme

Response surface methodology (RSM) is a statistical method based on the multivariate non-linear model that has been widely utilized in optimizing the operating variables. A mathematical model, which can best fit the experimental data, is developed, and the optimums of operating variables that generate a maximum or minimum response can be obtained by using this model [1].

Based on the BOX-Benhnken design and conducted by Design-Expert software it was used to design the experimental scheme. CuO-MnO content (10-30%), CeO_2 content (0.5-4.5%), calcination temperature (500-700 °C) and calcination time (4-8 h) were used as the independent variables, and the average carbon conversion rate within half an hour ($X_{c\text{-}0.5h}$) and the average carbon conversion rate within four hours ($X_{c\text{-}4h}$) were used as the response values. Therefore, 27 experimental points of response surface experiments were designed with four factors and three levels (Table 1).

In this experiment, $X_{c\text{-}0.5h}$ was used to characterize the activity of the catalyst, and $X_{c\text{-}4h}$ was used to characterize the stability of the catalyst. Since some of the catalysts had deactivated within four hours, the average conversion before deactivation was used to replace the average carbon conversion within four hours.

4. Catalyst Characterization Methods

X-ray Diffraction (XRD, Ultima VI, Japan) was performed at a setting of 40 kV and 40 mA (Cu Kα source) to determine the chemical composition and size of the actives. 2θ starts from 20° to 80° at 1°/min with a step of 0.02°.

X-ray Fluorescence (XRF, ARL Perform'X 4200) was performed to determine the sample composition.

Electron scanning microscope (FEI Inspect F50 scanning electron microscope, made by FEI, China) was used to study the surface topography structure changes before and after the reaction of different catalysts. The surface of the catalyst was cleaned and gold sprayed prior to scanning. This will result in better image quality.

Temperature-programmed reduction (TPR) was conducted to investigate the influences of active metal content and calcination conditions on the Cu-Mn-Ce catalysts. Catalyst samples (30 mg) were loaded in a quartz U-tube and evaluated in a PCA-1200 Chem-

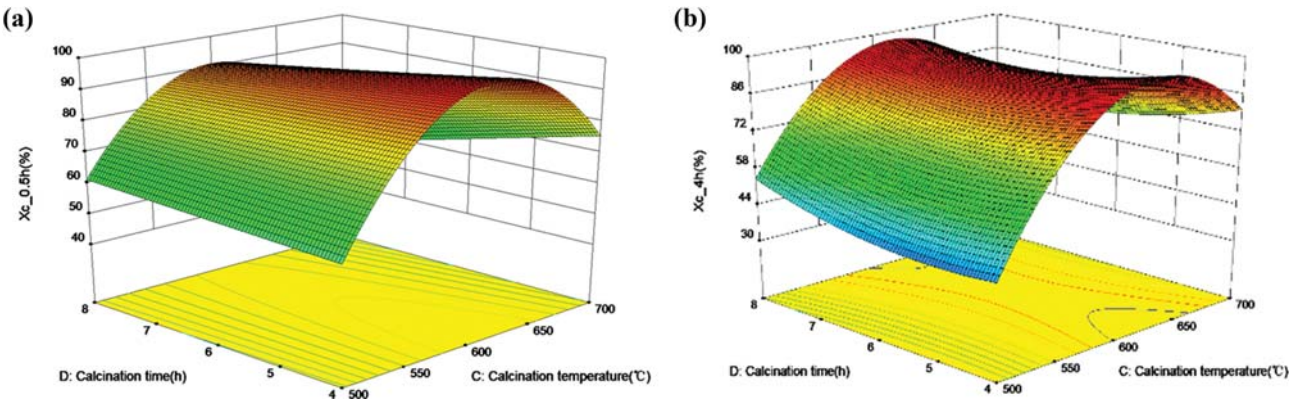

Fig. 1. Effects of calcination time and temperature on $X_{c\text{-}0.5h}$ and $X_{c\text{-}4h}$. (a) $X_{c\text{-}0.5h}$, (b) $X_{c\text{-}4h}$.

Table 2. Polynomial equations of $X_{c\text{-}0.5h}$ and $X_{c\text{-}4h}$

Response	Polynomial equation
$X_{c\text{-}0.5h}$	$57.94+25.31\ X_1+8.83\ X_2-17.14\ X_3+9.36\ X_2\ X_3-6.11\ X_3\ X_4+8.85\ X_1^2+4.70\ X_2^2$ $-4.14\ X_1^2\ X_4-10.91\ X_1\ X_2^2-25.74\ X_1\ X_3^2+23.23\ X_2^2\ X_3-9.34\ X_2\ X_3^2$
$X_{c\text{-}4h}$	$45.25+24.88\ X_1+7.76\ X_2-10.31\ X_3+4.84\ X_1\ X_2+4.56\ X_1\ X_3+8.52\ X_2\ X_3-5.82\ X_3\ X_4$ $+10.31\ X_1^2+7.31\ X_2^2+5.39\ X_4^2-7.14\ X_1\ X_2^2-26.81\ X_1\ X_3^2+16.12\ X_2^2\ X_3-9.72\ X_2\ X_3^2$

isorption Analyzer (Biaode, China). Fresh catalysts were prepared at 200 °C for 90 min in 30 ml/min of He and then cooled below 50 °C. A constant flow of 10% H_2/Ar was injected as the temperature ramped at 10 °C/min to 800 °C and held for 5 min.

X-ray photoelectron spectroscopy (XPS) was used in this study to analyze the valence state of the metal species and the presence of oxygen in the catalyst. The test instrument is a PHI Quantera II X-ray photoelectron spectrometer (Japan Nippon Nano Surface Analytical Instruments Co., Ltd.) with an aluminum target, XPS sensitivity >15 kcps, and energy resolution <0.60 eV.

5. Data Processing

In the reactor, the reaction occurred as shown in Eq. (1):

$$C_6H_6+7.5O_2\rightarrow 6CO_2+3H_2O \quad (1)$$

In the product gas, the gas components were CO_2, O_2, and N_2. Since N_2 was not consumed in this reaction, the volume of N_2 was constant before and after the reaction. The total volume after the reaction could be determined by N_2. During the experiment, the carbon conversion rate could be calculated using the simplified Eq. (2):

$$X_c=\frac{V_{CO_2}\times Mm}{22.4\times V_{ben}\times\rho\times No_{ben}}\times 100\% \quad (2)$$

where V_{CO_2} (L/min) was gas flow of CO_2 in the purified product gas, Mm was relative molecular mass of benzene (Mm=78), V_{ben} (ml/min) was benzene feed flow, ρ was the feed density of benzene (g/ml), and No_{ben} was the number of carbon atoms in each molecule of benzene (No_{ben}=6).

RESULTS AND DISCUSSION

1. Experimental Results

Experimental design and the corresponding results are presented in Table 1. To ensure that the experiments are repeatable, the repeated experiments were carried out under the condition with mean values of operation variables for five times (Case 1, Case 8, Case 15, Case 23, and Case 26), whose results showed good repeatability.

Multivariate regression was performed based on the data in Table 1. The mass fraction of CuO-MnO (%), the mass fraction of CeO_2 (%), the calcination temperature (°C), and the calcination time (h) are denoted as A, B, C, and D, respectively. The coefficients of D, AD, and CD, etc. in the regression model were small, and the *p*-value was very large (greater than 0.1, meaning a non-significant term), which leads to big differences between variance and the prediction variance of the model. Therefore, these items were removed in the model. The response surface is established after removing the non-significant items (not shown here; see Supplementary Data Table 2). On account of the analysis of variance (ANOVA), some statistical conclusions can be obtained as follows: (i) *p*-values of all the models are far less than 0.01, which indicates remarkable significance and reliability of the models, (ii) the R^2 values of $X_{c\text{-}0.5h}$ and $X_{c\text{-}4h}$ illustrate that the two models can explain 95.8% and 92.3% changes in the experiment; furthermore (iii) Adj-R^2 values of the two models are 0.93 and 0.95, further demonstrating the model reliability, (iv) Pre-R^2 and Adj-R^2 values are less than 0.2, indicating they are matched; moreover (v) lack-of-fit and Adeq precision are performed to study the impact of noise on signal, where the p values of lack-of-fit are greater than 0.05 and the Adeq precision values are no less than 4, indicating the little effect noise and the feasibility of two models to navigate the design space; eventually (vi) the error values of the two models are less than 7.2% and 6.7%, respectively, which are within acceptable limits.

2. Analysis of Response Surface

It is assumed that X_1=(A-20)/10, X_2=(B-2.5)/2, X_3=(C-600)/100 and X_4=(D-6)/2 to standardize the mass fraction of CuO-MnO

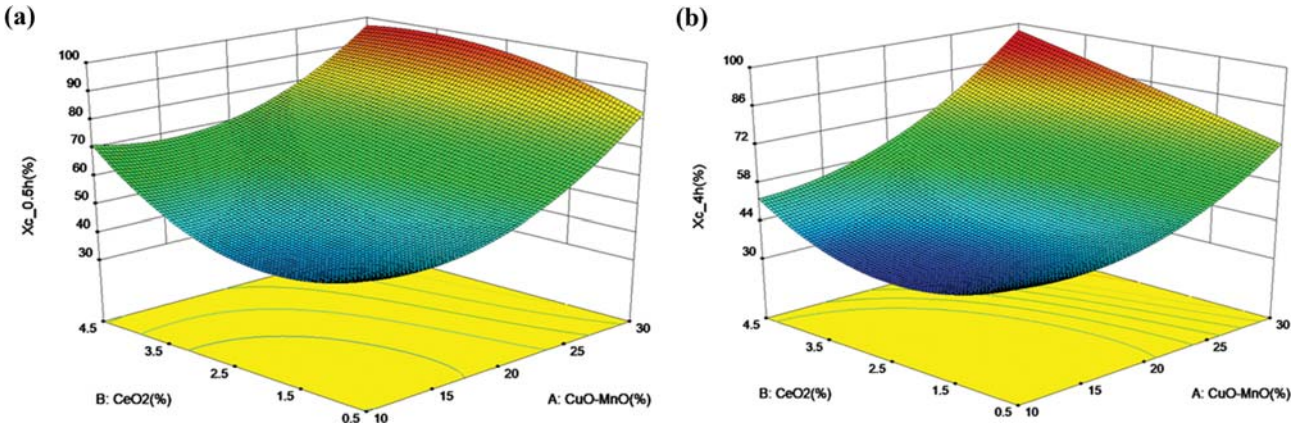

Fig. 2. Effects of active metal content on $X_{c\text{-}0.5h}$ and $X_{c\text{-}4h}$. (a) $X_{c\text{-}0.5h}$, (b) $X_{c\text{-}4h}$.

(%), CeO_2 (%), the calcination temperature (°C) and time (h), respectively. The relationship between the response values of $X_{c\text{-}0.5h}$ and $X_{c\text{-}4h}$, and operating variables is obtained by fitting multiple regression equations, as shown in Table 2.

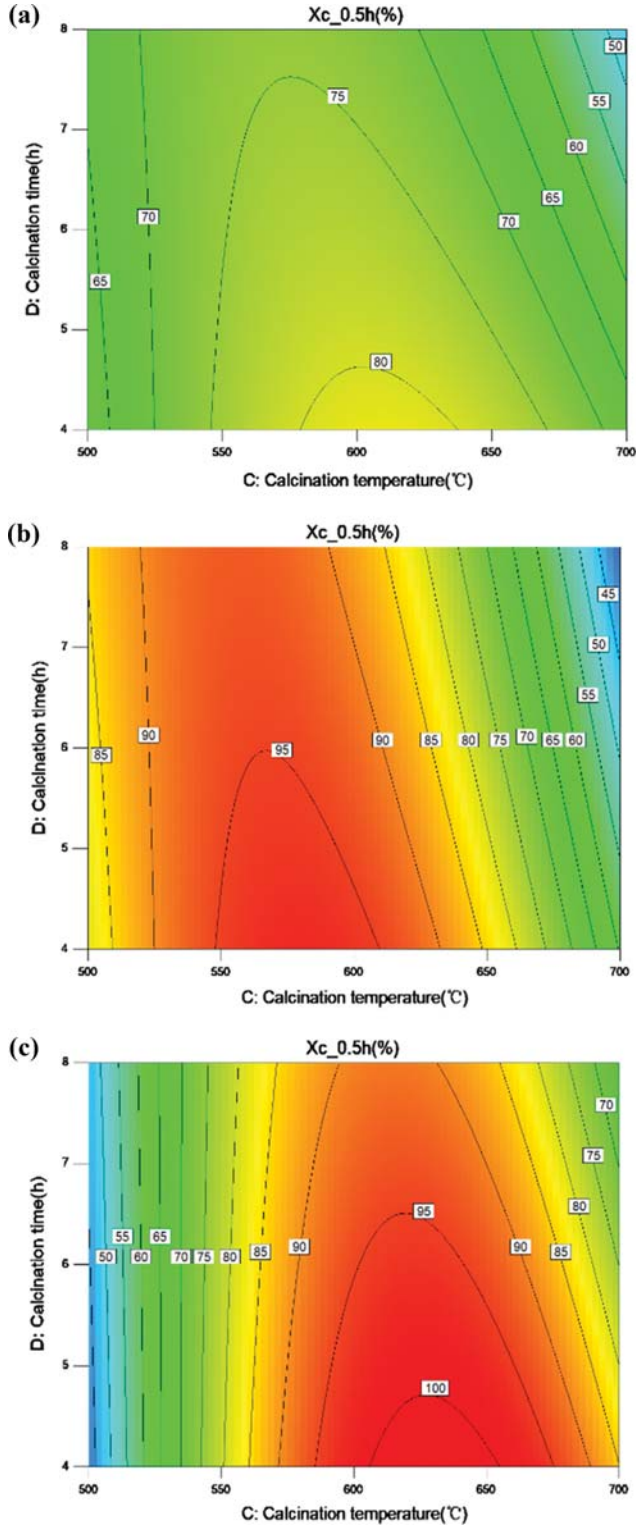

Fig. 3. Effect of CeO_2 content on $X_{c\text{-}0.5h}$. (a) 0.5% CeO_2, (b) 2.5% CeO_2, (c) 4.5% CeO_2.

2-1. Influence of Preparation Parameters

The effects of calcination conditions and active metal content on catalyst activity can be explored based on Design-Expert software and the polynomial equations in Table 2. Fig. 1 presents the effects of calcination time and temperature on the activities of the catalysts with 30% CuO-MnO and 4% CeO_2. It can be found that both $X_{c\text{-}0.5h}$ and $X_{c\text{-}4h}$ increase firstly and then decrease with increasing temperature, and the highest conversion rate of benzene is at around 600 °C. However, the calcination time only has a small effect on the catalyst activity. It can be seen that the high calcina-

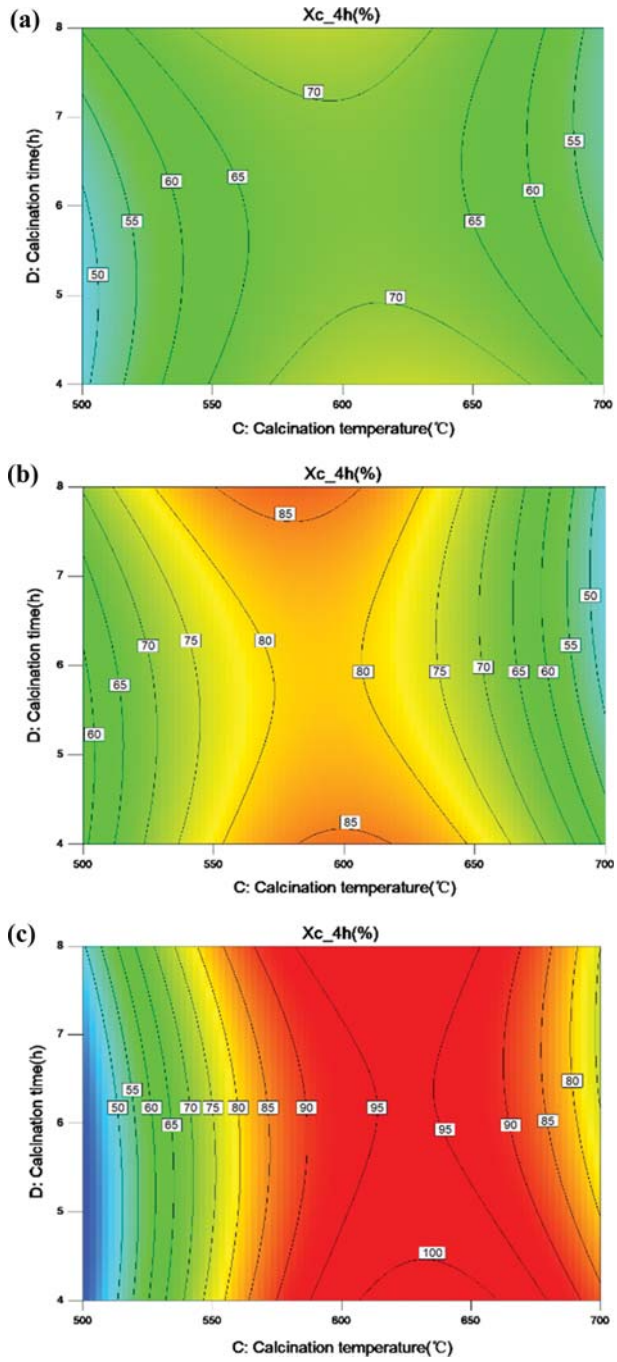

Fig. 4. Effect of CeO_2 content on $X_{c\text{-}4h}$. (a) 0.5% CeO_2, (b) 2.5% CeO_2, (c) 4.5% CeO_2.

tion temperature with short calcination time, whereas low calcination temperature with long calcination time, will lead to better catalyst performance. Catalysts with other content of CuO-MnO and CeO_2 also present the same trend. As shown in Fig. 2, when the calcination temperature and time of the catalyst are at 600 °C for 4 h, both $X_{c\text{-}0.5h}$ and $X_{c\text{-}4h}$ increase with the content of CuO-MnO and CeO_2 rising. $X_{c\text{-}0.5h}$ is enhanced significantly with the increase of CeO_2 when CuO-MnO content is at lower values. However, a slight decrease exists with the increase of CeO_2 when CuO-MnO content is close to 30%. Specific reasons are in the BET analysis (section 3.4.1).

Fig. 3 and Fig. 4 show $X_{c\text{-}0.5h}$ and $X_{c\text{-}4h}$ contours when CuO-MnO content is 30% with different CeO_2. The optimal temperatures for catalyst performance are all around 600 °C, which is little affected by the change of CeO_2 content. However, the maximum conversion rate shows a different trend as the CeO_2 content changes. As the CeO_2 content increases, the maximum $X_{c\text{-}0.5h}$ value increases rapidly and then slowly. According to the polynomial equations in Table 2, when the CeO_2 content is in the range of 0.5%-2.5% and the range of 2.5%-4.5%, the maximum values of $X_{c\text{-}0.5h}$ increase by 18.5% and 3.9%, respectively. For $X_{c\text{-}4h}$, the maximum values of $X_{c\text{-}4h}$ increase almost linearly by 16.7% with CeO_2 content rising. It indicates that the CeO_2 content has a more important influence on $X_{c\text{-}4h}$ than $X_{c\text{-}0.5h}$.

2-2. Optimization Condition for Catalyst Preparation

The experimental results show that $X_{c\text{-}0.5h}$ and $X_{c\text{-}4h}$ of 30-2.5-600-4 are 98.8% and 92.6%, respectively, and $X_{c\text{-}0.5h}$ and $X_{c\text{-}4h}$ of 30-4.5-600-6 are 95.6% and 91.4%, respectively. The optimal value of the response surface also appears in this neighborhood. To predict the optimal condition for catalyst preparation, the optimization of the numerical module is used to find a suitable combination of CuO-MnO mass fraction (%), CeO_2 mass fraction (%), calcination temperature (°C) and calcination time (h). The predicted results show that when the content of CuO-MnO and CeO_2 is 30% and 4.4%, respectively, and the calcination condition is 620 °C for 4.1 h, both $X_{c\text{-}0.5h}$ and $X_{c\text{-}4h}$ can reach 100%. A verification experiment was performed based on this scheme. The actual experimental results show that $X_{c\text{-}0.5h}$ and $X_{c\text{-}4h}$ are 99.5% and 97.1%, respectively, with the relative errors of which are 0.5% and 2.9% compared to the predicted values, respectively. It indicates that the optimization results are reasonable.

3. Effect of CuO-MnO and CeO_2 Contents on Catalytic Activity and Stability

Based on the experimental results of RSM, five cases were selected to analyze the effect of preparation conditions on the activity and stability of the catalyst: Case 3 (30-4.5-600-6), Case 4 (30-2.5-600-4), Case 24 (20-2.5-500-4), Case 25 (30-0.5-600-6), and Case 28 (20-4.5-600-4). The catalytic activity of the five catalysts within four hours is shown in Fig. 5. Catalyst 30-0.5-600-6 has high activity with X_c of 94.1% in the first 10 minutes. However, the catalytic activity decreases rapidly as reaction time further increases. During the period of 15-20 min, the average X_c is 63.8%. And in the next 220 min, X_c still keeps at around 65%, which exhibits a rapid decline at first and then a stable state in the catalytic activity. For catalyst 30-2.5-600-4, X_c can reach almost 100% at the beginning of the reaction, and it can remain more than 90% before 180 min. However, X_c decreases significantly to 85.2% at 180 min, and it can remain 81.9% to the end of the reaction, which shows the performance of slow deactivation. For catalyst 30-4.5-600-6, $X_{c\text{-}0.5h}$ and $X_{c\text{-}4h}$ are 95.6% and 91.4%, respectively, exhibiting the best catalytic activity and stability within four hours, which indicates the performance of long-term high efficiency and stability.

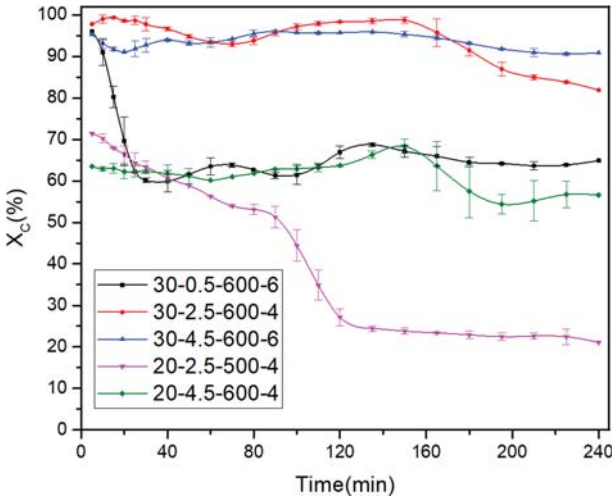

Fig. 5. Carbon conversion rate with reaction time.

It can be found that the catalytic activity of three catalysts (30-4.5-600-6, 30-2.5-600-4 and 30-0.5-600-6) has great differences within four hours. The previous response surface analysis shows that the calcination time has few effects on the catalyst activity, hence the difference is mainly caused by the CeO_2 content. It can be seen that $X_{c\text{-}0.5h}$ increases with the CeO_2 content increasing, but $X_{c\text{-}0.5h}$ is nearly unchanged when the CeO_2 content is higher than 2.5%. However, when the reaction time is longer than 180 min, the values of X_c exhibit a significant difference for the three catalysts, which are 64.4%, 81.9%, and 90.9%, respectively, at the 240th min of reaction. It implies that the increase of CeO_2 can improve catalyst stability.

As shown in Fig. 5, when the CuO-MnO content decreases to 20%, the values of $X_{c\text{-}0.5h}$ of both 20-2.5-500-4 and 20-4.5-600-4 catalysts reduce to around 65%, indicating that the CuO-MnO content has an important effect on the catalytic activity. However, there is a great difference in X_c of the two catalysts for a long time reaction. For catalyst 20-4.5-600-4, X_c fluctuates slightly, which keeps at around 60% within 4h, but X_c of catalyst 20-2.5-500-4 decreases significantly to 25% after 110 min. Additionally, the other catalysts calcined at 500 °C (Case 6, Case 9, Case 11, Case 20, Case 24) also show rapid deactivation. It indicates that the low calcination temperature (500 °C) of catalyst results in poor stability.

4. Catalyst Characterization

4-1. BET Analysis

The BET analysis of the Cu-Mn-Ce catalysts is shown in Table 3. The catalysts are prepared using the vacuum impregnation method so that the specific surface area will decrease with the increasing of the metal content. On one hand, the increase of CeO_2 results in the decrease of the specific surface area to weaken the adsorbed capacity of the catalyst. On the other, the increase of CeO_2

Table 3. The specific surface area and pore volume of catalyst

Catalyst	Specific surface area (m/g)	Pore volume (cm^3/g)
30-0.5-600-6	130	0.38
30-2.5-600-4	118	0.35
30-4.5-600-6	109	0.33

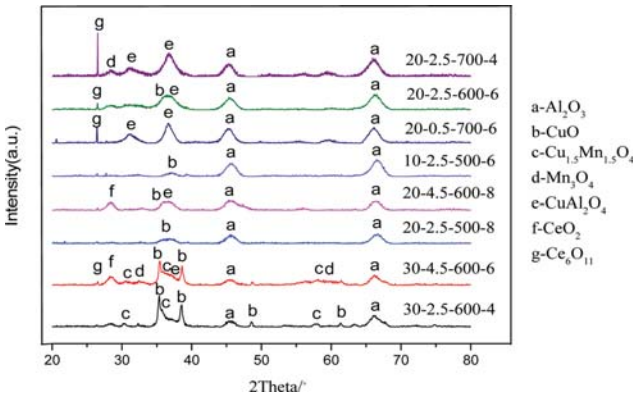

Fig. 6. XRD patterns of the catalysts.

enhances the rate of oxide transfer to improve the catalytic activity. Therefore, there exists the optimum content of CeO_2 for the different CuO-MnO. So Fig. 2 shows that a slight decrease exists with the increase of CeO_2 when CuO-MnO content is close to 30%.

4-2. XRD Analysis

The XRD patterns of the Cu-Mn-Ce catalysts and the main crystalline substances are shown in Fig. 6. In the catalyst, Cu exists in the form of CuO, $CuAl_2O_4$, and $Cu_{1.5}Mn_{1.5}O_4$, mainly in the form of CuO and $CuAl_2O_4$. Mn mainly exists in the form of $Cu_{1.5}Mn_{1.5}O_4$ and Mn_3O_4, and Mn can only be detected when CuO-MnO content is 30% because the content of Mn is low in other catalysts.

The form of Cu is highly correlated with the calcination temperature and calcination time. When the calcination temperature is 700 °C, the content of $CuAl_2O_4$ in the catalyst increases significantly. The main active metal exists as CuO when the calcination temperature is 500 °C and 600 °C. When the calcination temperature is 600 °C, a part of $CuAl_2O_4$ forms, because the long calcination time and high calcination temperature result in enhancing the interaction between the active metal and the carrier. When the content of CuO-MnO is 30%, $Cu_{1.5}Mn_{1.5}O_4$ appears at 2θ=30.36°, 35.86° and 57.62°. However, $Cu_{1.5}Mn_{1.5}O_4$ cannot be detected as CuO-MnO decrease because $Cu_{1.5}Mn_{1.5}O_4$ forms less. Siham [30] found

Table 4. The particle sizes of CuO and $Cu_{1.5}Mn_{1.5}O_4$

Catalyst	Crystal phase	Size (nm)
30-0.5-600-6	CuO	14.2
	$Cu_{1.5}Mn_{1.5}O_4$	12.8
30-2.5-600-4	CuO	12.7
	$Cu_{1.5}Mn_{1.5}O_4$	8.5
30-4.5-600-6	CuO	9.5
	$Cu_{1.5}Mn_{1.5}O_4$	6.5

that the $Cu_{1.5}Mn_{1.5}O_4$ with spinel structure was better than CuO, which implies that $Cu_{1.5}Mn_{1.5}O_4$ makes the benzene easily oxidized. Therefore, the formation of $Cu_{1.5}Mn_{1.5}O_4$ is beneficial in enhancing the performance of the catalyst.

Ce in the catalyst exists in the form of CeO_2 and Ce_6O_{11}. CeO_2 can only be detected when CeO_2 content reaches 4.5% among these catalysts. When the calcination temperature is 700 °C, the peak intensity of Ce_6O_{11} is high, but a low temperature leads to a weak intensity. The reason is that the crystal grains grow and aggregate, rapidly forming a large crystal at a higher calcination temperature, whereas Ce_6O_{11} has a higher dispersion with a weaker peak at a lower temperature. The particle sizes of CuO and $Cu_{1.5}Mn_{1.5}O_4$ can be roughly estimated by Scherrer formula: $D_c=0.89\lambda/B\cos(\theta)$, where λ is copper target wavelength (0.15406 nm), B is full width at half maxima and θ is diffraction angle. The particle sizes of CuO and $Cu_{1.5}Mn_{1.5}O_4$ can be roughly estimated by Scherrer formula: $D_c=0.89\lambda/B\cos(\theta)$, where λ is copper target wavelength (0.15406 nm), B is full width at half maxima and θ is diffraction angle. The particle sizes of catalyst with different contents of CeO_2 are shown in Table 4. When the content of CeO_2 in the catalyst increases, the particle sizes of both CuO and $Cu_{1.5}Mn_{1.5}O_4$ decrease significantly. It indicates that the increase of CeO_2 content improves the dispersion of the crystal phase.

4-3. XRF Analysis

The element content in catalysts was analyzed using XRF (Table 5). As shown, the measured values are consistent with the theoretical values. The reason that Mn and Ce are difficult to detect in XRD analysis (Section 3.4.2) may be due to the low ratio and high dispersion.

4-4. H_2-TPR Analysis

To characterize reducibility, the catalyst was analyzed by H_2-TPR. As shown in Fig. 7, all catalysts have two distinct overlap peaks. When the calcination temperature is 600 °C, the first peak is at 208-215 °C and the second is at 236-246 °C. Combined with

Table 5. XRF analysis results

	30-0.5-600-6		30-4.5-600-6		20-0.5-600-6	
	Measured value (wt%)	Theoretical value (wt%)	Measured value (wt%)	Theoretical value (wt%)	Measured value (wt%)	Theoretical value (wt%)
Al	34.95	36.79	34.08	34.68	38.24	42.09
Cu	17.71	18.06	17.19	18.06	12.39	12.04
Mn	5.33	5.17	5.12	5.17	3.34	3.45
Ce	0.41	0.41	3.56	3.66	0.39	0.41

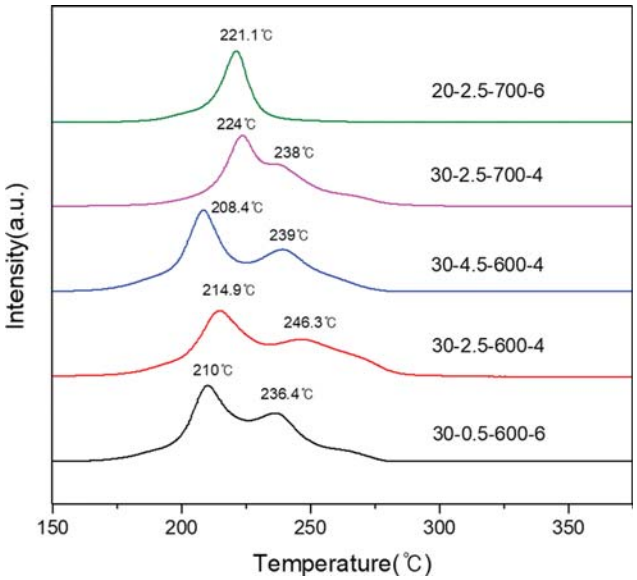

Fig. 7. Effects of CeO_2 and calcination temperature on the reduction ability of the catalyst.

the literature [44] and XRD analysis, the two peaks correspond to the stepwise reduction of CuO. Thus, the first peak of H_2 consumption is related to the Cu^{2+} to Cu^{+1} step and the second peak to the Cu^{+1} to Cu^0. It is reported that the pure CuO profile exhibits a single reduction peak centered at ~250 °C, and the peak temperature can be lower by modifying Mn or Ce [30,44-47]. This study also indicates that interaction between copper oxide and cerium oxide as well as manganese oxide enhance the catalytic ability of CuO, which is consistent with the previous works. The reduction peak will be affected by CeO_2 content, catalyst specific surface area, and particle size. However, the peak of Mn_3O_4 is not shown in Fig. 7, which may result from the low concentration of Mn and overlapping with the peak of CuO. The reduction peak temperature of Mn_3O_4 is lowered due to the interaction of active metal.

When the calcination temperature is 700 °C, the reduction peaks delay to 224 °C and 238 °C, and the peak area of catalyst 30-2.5-700-6 is reduced by 25% compared to catalyst 30-2.5-600-4. Because calcination at 700 °C causes the active metal particles to become larger and the active sites correspondingly decrease. This indicates that the increase in the calcination temperature results in a poor change in the active metal and a decrease in the number of active sites. When the CuO-MnO is 20%, one peak (221 °C) can only be observed. The peak area of catalyst 20-2.5-700-6 is reduced by 42% compared to catalyst 30-2.5-700-4. This indicates that the decrease in CuO-MnO will lead to a decrease of active sites. Therefore, it will weaken the catalytic ability.

4-5. SEM Analysis

The catalyst is characterized by SEM to indicate the change of catalyst surface morphology before and after the reaction. The morphology of catalyst 30-0.5-600-6 (not shown here; see the Supplementary Data Fig. 2) and 30-4.5-600-6 (not shown here; see the Supplementary Data Fig. 3) has no obvious change, although both catalysts exhibit different catalytic stability. It indicates that the decrease in the catalytic ability of catalyst 30-0.5-600-6 is not due to the destruction of the surface structure. The fresh catalyst 20-2.5-500-4 (not shown here; see the Supplementary Data Fig. 4) appears as a sheet structure, and however, some agglomerations occur on the catalyst surface after the reaction. It implies that the sheet structure of CuO is weak, resulting in the fast deactivation of the catalyst. Furthermore, the surface lattice may migrate in the reaction because the Tammann temperature of CuO is around 240 °C. Especially, catalytic oxidation is an exothermic reaction, which likely causes the local over-temperature on the catalyst surface. Thus the crystal structure of the active metal is easily destructed in the oxidation reaction. It indicates that the low calcination temperature is the main reason for the insufficient structure strength of the catalyst.

The characterization of SEM indicates that the calcination conditions have a significant effect on the morphology and strength of the catalyst structure, especially for the calcination temperature, which influences the stability of the catalyst. For the test of $X_{c\text{-}0.5h}$ and $X_{c\text{-}4h}$, the different reaction time could bring about not only the different changes of the catalyst structure but also carbon deposition on the catalyst surface due to the difference in catalytic activities. Therefore, the conversion rates of benzene for $X_{c\text{-}0.5h}$ and $X_{c\text{-}4h}$ exhibit an obvious difference using the catalysts based on the different calcination conditions.

4-6. XPS Analysis

The catalyst is characterized by XPS to indicate the oxidation state of the catalyst surface substance. Fig. 8 shows the Mn 2p XPS spectra of the catalysts, in which Mn 2p doublet can be distinguished. The binding energy of Mn $2p_{1/2}$ appears at 653.3 eV, and the one of Mn $2p_{3/2}$ appears at 641.8 eV. According to the literature [26], the binding energy may correspond to Mn_2O_3. Also, the broad peak of Mn $2p_{3/2}$ is presented, which indicates that Mn^{2+} ions may coexist with Mn^{3+} ions at the surface of the catalysts [26].

Fig. 9 shows the Cu 2p XPS spectra of the catalysts. As shown, two main peaks can be observed, which are assigned to the binding energies of $2p_{1/2}$ and $2p_{3/2}$, respectively. The peak fitting result of Cu $2p_{3/2}$ for 30-4.5-600-4 catalyst is shown in Fig. 10. In the

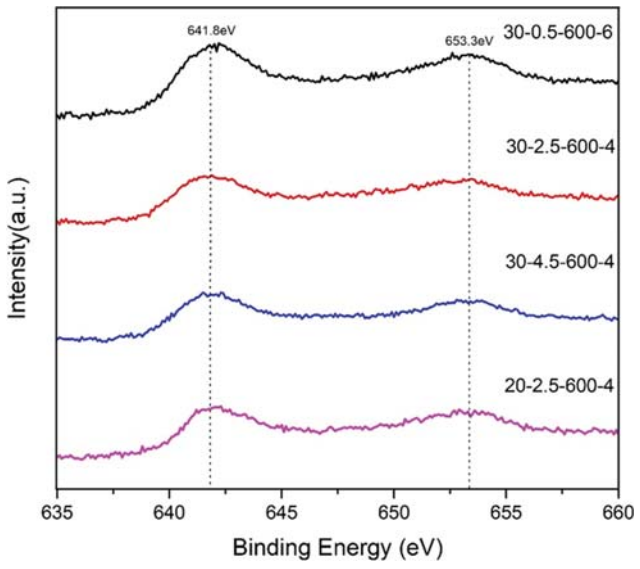

Fig. 8. XPS spectrum of catalyst Mn 2p.

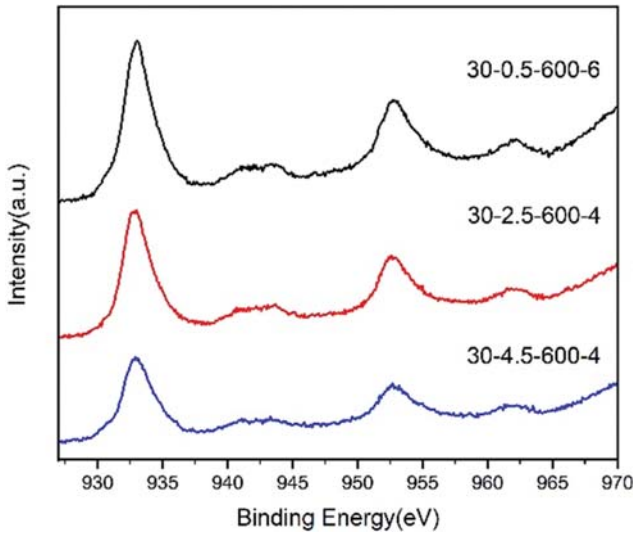

Fig. 9. XPS spectrum of catalyst Cu 2p.

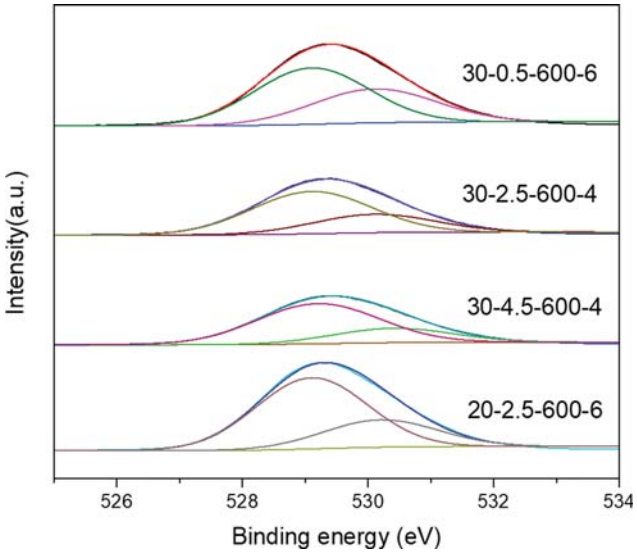

Fig. 11. XPS spectrum of catalyst O 1s.

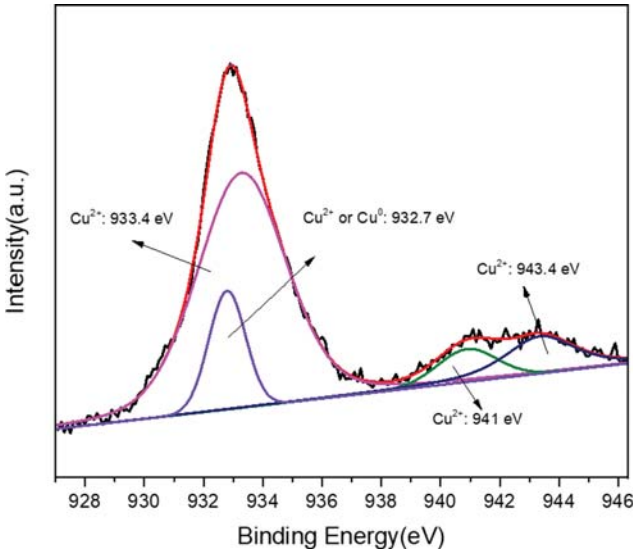

Fig. 10. Peak fitting of Cu $2p_{3/2}$ for 30-4.5-600-4 catalyst.

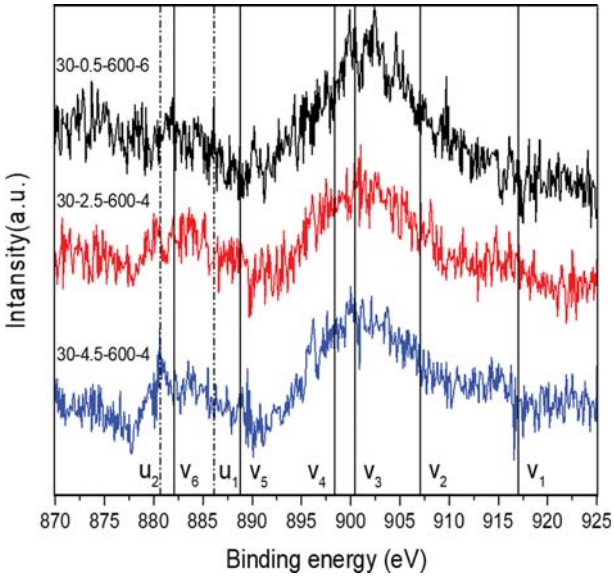

Fig. 12. XPS spectrum of catalyst Ce 3d.

main peak, the peak at 932.6 eV could represent the Cu^{+} or Cu^{0}, and the peak at 933.5 eV could represent the Cu^{2+}. Meanwhile, satellites located at 941.1 eV and 943.4 eV are observed, which are attributed to the Cu^{2+} [48]. Moreover, the ratio of the total Cu^{2+} on the surface of the catalyst 30-4.5-600-4 is 87% according to the peak area in XPS analysis. According to the Cu LMM spectra, Cu^{+} and Cu^{0} coexist on the surface of 30-4.5-600-4 catalyst, which is consistent with the literature [11].

Fig. 11 and Fig. 12 show the XPS spectrum of O 1s and Ce 3d on the catalysts. It can be seen from the spectrum that two oxygen species are detected. The peak at low binding energy (529.1 eV to 529.2 eV) represents the lattice oxygen (O_{lat}), and the peak at high binding energy (530.1 eV to 530.4 eV) represents the defect oxygen (O_{def}). As shown in Table 6, the increase of CeO_2 can significantly enhance the lattice oxygen ratio on the catalyst surface when the content of CuO-MnO is the same. Fig. 12 shows that six peaks

Table 6. The lattice oxygen and defect oxygen on the catalysts

Catalyst	BE(eV)		$O_{lat}/(O_{lat}+O_{def})$ (%)
	Lattice oxygen (O_{lat})	Defect oxygen (O_{def})	
30-0.5-600-6	529.1	530.1	60.6
30-2.5-600-4	529.1	530.1	69.5
30-4.5-600-4	529.2	530.4	74.2
20-2.5-600-6	529.1	530.2	71.7

of V_1 (916.7 eV), V_2 (907.3 eV), V_3 (900.8 eV), V_4 (898.3 eV), V_5 (888.6 eV), and V_6 (882.3 eV) are considered to be Ce^{4+} 3d status in the catalyst [26]. The characteristic peaks of Ce^{3+} can also be detected, which are at U_1 (885.8 eV) and U_2 (880.7 eV), respec-

tively. This indicates that there are two valence states of Ce^{4+} and Ce^{3+} in the catalyst. It is reported that oxygen vacancies are generated to maintain electronic balance when the Ce^{3+} appears, according to Eq. (3), where □ represents the oxygen vacancy [36]. The existence of the oxygen vacancy in the catalyst is beneficial to the transport of active oxygen. Thus the reduced active sites on the catalyst surface can be more easily oxidized [36].

$$4Ce^{4+}+2O^{2-}\rightarrow 4Ce^{4+}+2e^{-}/\square+0.5O_2\rightarrow 2Ce^{4+}+2Ce^{3+}+\square+0.5O_2 \quad (3)$$

According to the mechanism of catalytic oxidation-reduction [38], there are two steps as follows:

Step 1: The catalyst reacts with the tar leading to the reduction of activated metal sites on the catalyst and the oxidation of tar.

$$Tars+Cat-O\rightarrow Cat+CO_2 \quad (4)$$

Step 2: Oxygen molecules in the air oxidize the reduced activated metal sites resulting in the oxidation of the catalyst.

$$2Cat+O_2\rightarrow 2Cat-O \quad (5)$$

When CeO_2 is added to Cu-Mn based catalyst, the presence of oxygen vacancies promotes the activation and transport of active oxygen. During the oxidation reaction of benzene, the catalyst is reduced and oxidized simultaneously, maintaining the redox cycle. As the CeO_2 content increases, the number of oxygen vacancies in the catalyst rises correspondingly, and thus the rate of step 2 in the redox is accelerated. Literature [11] reports that the redox interaction between CuO and $Ce_{1-x}Mn_xO_2$ could induce the formation of Cu^+ at the interface. Moreover, the synergistic function induced by electronic transfer between Cu^{2+}/Ce^{4+} and Cu^{+}/Ce^{3+} endowed catalyst with excellent reducibility, and enhanced lattice oxygen mobility and utilization efficiency [22].

For the catalyst with a 30% concentration of CuO-MnO, CuO-MnO active metal can promote the reaction rate of step 1, which leads to the fast consumption of the active oxygen on the catalyst surface. When the catalyst contains merely 0.5% CeO_2, the rate of step 2 is slower due to insufficient oxygen vacancies, indicating that step 2 is the control step. Therefore, for catalyst 30-0.5-600-6, the surface active oxygen cannot be replenished in time and catalytic activity rapidly decreases at the beginning of the reaction.

The activities of catalyst 30-2.5 2.5-600-4 and 30-4.5-600-6 remain at a high level for a long time, which means the rate of step 2 is significantly improved with the CeO_2 increasing. Although catalyst 20-2.5-600-6 has relatively higher ratios of lattice oxygen and CeO_2, the performance of the catalyst with a small amount of CuO-MnO maintains a low level for a long time reaction, which indicates that step 1 is the control step. It implies that the different ratio of active substance and CeO_2 causes the change of the control step for the catalytic redox.

CONCLUSION

Based on the response surface methodology and catalyst characterization, the optimal preparation scheme of catalyst for benzene catalytic oxidation was sought and the influences of various factors on the catalyst activity were discussed. The following conclusions can be drawn:

1. Based on the response surface methodology, the optimum preparation condition of Cu-Mn-Ce catalyst for catalytic oxidation of benzene is CuO-MnO content of 30% and CeO_2 content of 4.4% at calcination temperature of 620 °C for 4.1 h.

2. The calcination temperature significantly affects the catalyst structure and type of the active metal. A lower calcination temperature tends to cause a weak structure strength, while a higher temperature results in decreasing the reducibility.

3. The main roles of CeO_2 on the catalyst are presented in two aspects. On one hand, CeO_2 increases the dispersion of the active metal and enhances the catalyst stability. On the other hand, the oxygen vacancies on catalyst are increased and the oxygen transfer ability is improved, thereby improving the oxidized ability of the catalyst.

4. In this study, the catalytic oxidization of benzene complied with MVK mechanism. The content of CuO-MnO determines the number of active sites on the catalyst, which promotes the reduction of catalyst. CeO_2 plays an important role in enhancing the oxidization of catalyst. Therefore, the ratio of CuO-MnO to CeO_2 in the catalyst will cause the change of the control step of the redox reaction.

ACKNOWLEDGEMENT

This work was supported by the National Natural Science Foundation of China (51576047).

SUPPORTING INFORMATION

Additional information as noted in the text. This information is available via the Internet at http://www.springer.com/chemistry/journal/11814.

REFERENCES

1. X. Lv, J. Xiao, L. H. Shen and Y. Y. Zhou, *Int. J. Hydrogen Energy*, **41**, 21913 (2016).
2. P. Haro, P. Ollero, A. L. V. Perales and F. Vidal-Barrero, *Biofuel. Bioprod. Bior.*, **7**, 551 (2013).
3. L. B. Yan, Y. Cao and B. S. He, *Chem. Eng. J.*, **331**, 435 (2018).
4. M. Aneke and M. H. Wang, *Energy Procedia*, **142**, 829 (2017).
5. S. Anis and Z. A. Zainal, *Renew. Sust. Energy Rev.*, **15**, 2355 (2011).
6. X. Lv, J. Xiao, T. T. Sun, X. D. Huo, M. Song and L. H. Shen, *Korean J. Chem. Eng.*, **35**, 394 (2018).
7. T. Miyazawa, T. Kimura, J. Nishikawa, S. Kado, K. Kunimori and K. Tomishige, *Catal. Taday*, **115**, 254 (2006).
8. G. Guan, M. Kaewpanha, X. Hao and A. Abudula, *Renew. Sust. Energy Rev.*, **58**, 450 (2015).
9. H. M. Xie, Q. X. Du, H. Li, G. L. Zhou, S. M. Chen, Z. J. Jiao and J. M. Ren, *Korean J. Chem. Eng.*, **34**, 1944 (2017).
10. S. S. Hong, G. H. Lee and G. D. Lee, *Korean J. Chem. Eng.*, **20**, 440 (2003).
11. T. Y. Li, S. J. Chiang, B. J. Liaw and Y. Z. Chen, *Appl. Catal. B-environ.*, **103**, 143 (2011).
12. S. J. Yoon, Y. K. Kim and J. G. Lee, *Ind. Eng. Chem. Res.*, **50**, 2445 (2011).
13. W. X. Tang, Y. Z. Deng, W. H. Li, S. D. Li, X. F. Wu and Y. F. Chen,

Catal. Commun., **72**, 165 (2015).
14. T. B. Dorr, S. Schmidt, A. Drochner and H. Vogel, *Chem. Eng. Technol.*, **40**, 351 (2017).
15. Y. F. Wang, C. B. Zhang, F. D. Liu and H. He, *Appl. Catal. B-environ.*, **142**, 72 (2013).
16. Z. B. Rui, C. Y. Chen, Y. B. Lu and H. B. Ji, *Chin. J. Chem. Eng.*, **22**, 882 (2014).
17. C. He, J. Cheng, X. Zhang, M. Douthwaite, S. Pattisson and Z. P. Hao, *Chem. Rev.*, **119**, 4471 (2019).
18. M. S. Kamal, S. A. Razzak and M. M. Hossain, *Atmos. Environ.*, **140**, 117 (2016).
19. S. C. Kim and W. G. Shim, *Appl. Catal. B-environ.*, **92**, 429 (2009).
20. T. Tabakova, L. Ilieva, P. Petrova, A. M. Venezia, G. Avdeev, R. Zanella and Y. Karakirova, *Chem. Eng. J.*, **260**, 133 (2015).
21. I. H. Son, A. M. Lane and D. T. Johnson, *J. Power Sources*, **124**, 415 (2003).
22. J. Lin, Y. F. Guo, C. H. Li, S. X. Lu, X. Chen and K. M. Liew, *Catal. Lett.*, **148**, 2348 (2018).
23. D. S. Wang and Y. D. Li, *J. Am. Chem. Soc.*, **132**, 6280 (2010).
24. F. Wang and G. X. Lu, *Int. J. Hydrogen Energy*, **35**, 7253 (2010).
25. Z. Y. Jiang, X. B. Feng, J. L. Deng, C. He, M. Douthwaite, Y. K. Yu, J. Liu, Z. P. Hao and Z. Zhao, *Adv. Funct. Mater.*, **29**, 2230 (2019).
26. Z. Wang, G. L. Shen, J. Q. Li, H. D. Liu, Q. Wang and Y. F. Chen, *Appl. Catal. B-environ.*, **138**, 253 (2013).
27. C. He, Y. K. Yu, L. Yue, N. L. Qiao, J. J. Li, Q. Shen, W. J. Yu, J. S. Chen and Z. P. Hao, *Appl. Catal. B-environ.*, **147**, 156 (2014).
28. S. C. Kim, Y. K. Park and J. W. Nah, *Powder Technol.*, **266**, 292 (2014).
29. A. Aziz, M. Sajjad, S. Kim, M. Saifuddin and K. S. Kim, *Appl. Sci-Basel*, **8**, 1920 (2018).
30. S. Behar, P. Gonzalez, P. Agulhon, F. Quignard and D. Swierczynski, *Catal. Taday*, **189**, 35 (2012).
31. P. Yang, J. R. Li and S. F. Zuo, *Chem. Eng. Sci.*, **162**, 218 (2017).
32. Y. F. Guo, C. W. Zhao, J. Lin, C. H. Li and S. X. Lu, *Catal. Commun.*, **99**, 1 (2017).
33. J. Lin, Y. F. Guo, X. Chen, C. H. Li, S. X. Lu and K. M. Liew, *Catal. Lett.*, **148**, 181 (2018).
34. J. Li, Q. Li, X. Chen, C. H. Li, S. X. Lu and K. M. Liew, *Chem. Eng. J.*, **371**, 267 (2019).
35. M. Koike, C. Ishikawa, D. L. Li, L. Wang, Y. Nakagawa and K. Tomishige, *Fuel*, **103**, 122 (2013).
36. X. W. Liu, K. B. Zhou, L. Wang, B. Y. Wang and Y. D. Li, *J. Am. Chem. Soc.*, **131**, 3140 (2009).
37. B. Li, Y. W. Chen, L. Li, J. W. Kan, S. He, B. Yang, S. B. Shen and S. M. Zhu, *J. Mol. Catal. A-chem.*, **415**, 160 (2016).
38. H. H. Chen, Y. Yan, Y. Shao, H. P. Zhang and H. H. Chen, *AIChE J.*, **61**, 620 (2015).
39. A. Z. Abdullah, M. Z. Abu Bakar and S. Bhatia, *Ind. Eng. Chem. Res.*, **42**, 6059 (2003).
40. H. Li, H. Chen, M. F. Yao and Y. D. Li, *Ind. Eng. Chem. Res.*, **52**, 686 (2013).
41. C. I. Meyer, A. Borgna, A. Monzon and T. F. Garetto, *J. Hazard. Mater.*, **190**, 903 (2011).
42. S. Behar, N. A. Gomez-Mendoza, M. A. Gomez-Garcia, D. Swierczynski, F. Quignard and N. Tanchoux, *Appl. Catal. A-gen.*, **504**, 203 (2015).
43. X. D. Huo, J. Xiao, M. Song and L. Zhu, *J. Anal. Appl. Pyrol.*, **135**, 189 (2018).
44. F. Marino, B. Schonbrod, M. Moreno, M. Jobbagy, G. Baronetti and M. Laborde, *Catal. Taday*, **133**, 735 (2008).
45. H. J. Zhao, K. G. Fang, J. Zhou, M. G. Lin and Y. H. Sun, *Int. J. Hydrogen Energy*, **41**, 8819 (2016).
46. D. Delimaris and T. Ioannides, *Appl. Catal. B-environ.*, **89**, 295 (2009).
47. X. C. Zheng, X. L. Zhang, X. Y. Wang, S. R. Wang and S. H. Wu, *Appl. Catal. A-gen.*, **295**, 142 (2005).
48. J. Li, Z. L. Zhang, Y. J. Ji, Z. Y. Jin, S. Y. Zou, Z. Y. Zhong and F. B. Su, *Nano Res.*, **9**, 1377 (2016).

Supporting Information

Catalytic oxidation of benzene over alumina-supported Cu-Mn-Ce mixed oxide catalysts

Yang Gao, Jun Xiao†, Jiandong Ye, Xiaodong Huo, and Yutong Shen

Key Laboratory of Energy Thermal Conversion and Control of Ministry of Education, School of Energy and Environment, Southeast University, Nanjing, China
(*Received 17 July 2019 • accepted 12 November 2019*)

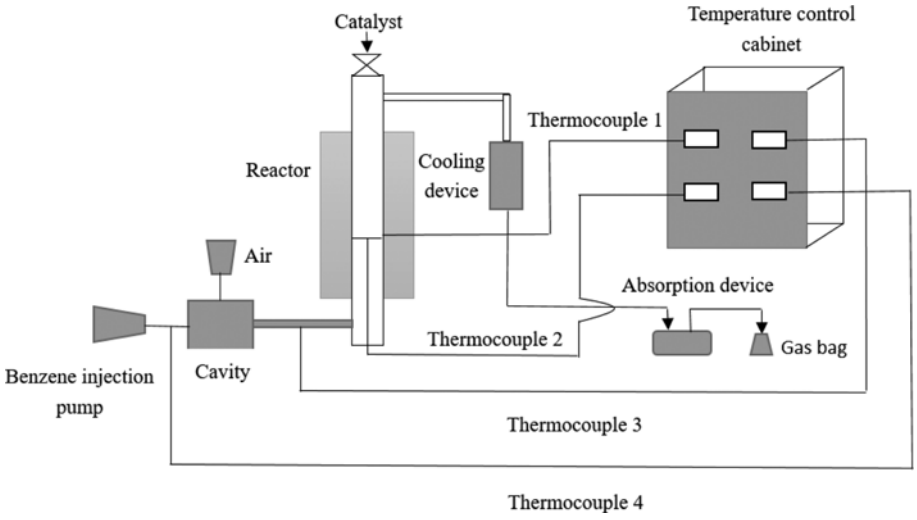

Fig. 1. Experimental system for catalytic oxidation of benzene.

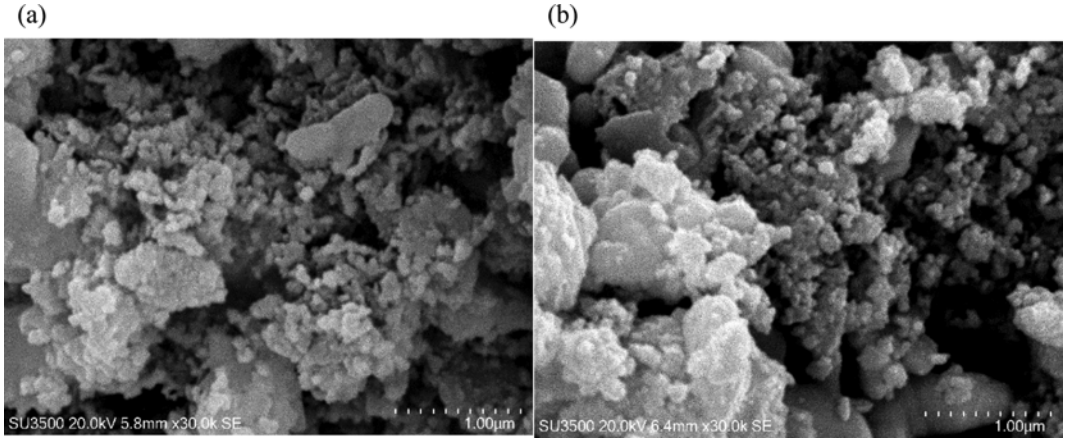

Fig. 2. Morphology change of 30-0.5-600-6 catalyst. (a) Befor experiment, (b) after experiment.

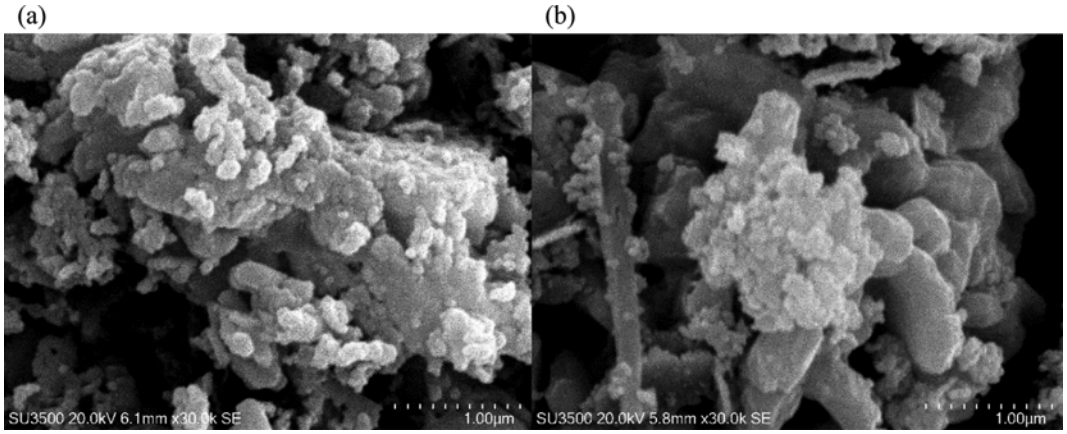

Fig. 3. Morphology change of 30-4.5-600-6 catalyst. (a) Before experiment, (b) after experiment.

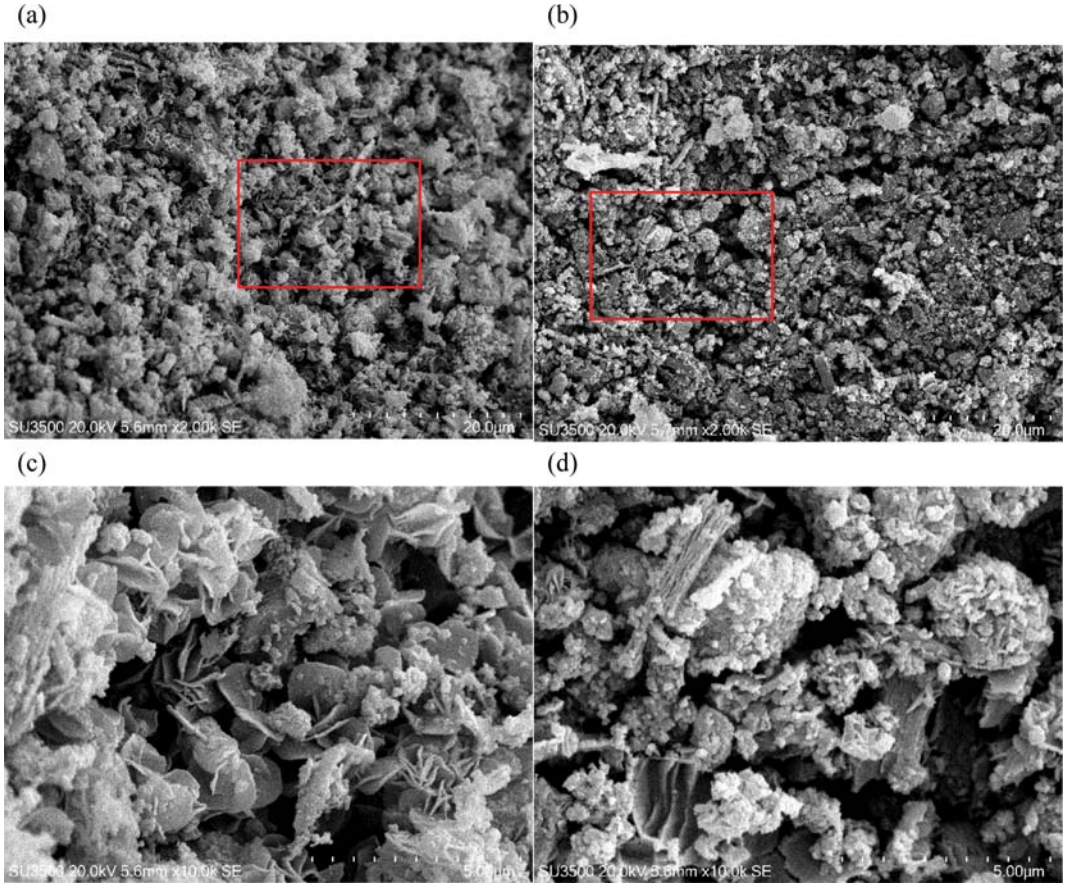

Fig. 4. Morphology change of 20-2.5-500-4 catalyst. (a), (c) Before experiment, (b), (d) after experiment.

Table 1. Detailed information of the aqueous solution

Reagent	Manufacturer	Class
$Cu(NO_3)\cdot 6H_2O$	Chengdu West Asia Chemical Co., Ltd., China	GR
$Mn(NO_3)_2$	Chengdu Kelon Chemical Reagent Factory, China	AR
$Ce(NO_3)_3\cdot 6H_2O$	Nanjing Chemical Reagent Co., Ltd., China	AR
Benzene	Chengdu Kelon Chemical Reagent Factory, China	AR

Table 2. Variance analysis of the response models

Response variables	$X_{c\text{-}0.5h}$				Response variables	$X_{c\text{-}4h}$			
	Coefficient	Sum of squares	DF	p-Value		Coefficient	Sum of squares	DF	p-Value
Model		7710.3	12	0.000	Model		6833.54	14	0.000
A	25.31	2562.69	1	0.000	A	24.88	2475.51	1	0.000
B	8.83	624.06	1	0.000	B	7.76	481.86	1	0.000
C	−17.14	2350.1	1	0.000	C	−10.31	849.75	1	0.000
AB	9.36	350.57	1	0.001	AB	4.84	93.7	1	0.020
CD	−6.11	149.24	1	0.017	AC	4.56	83.27	1	0.027
A^2	8.85	540.33	1	0.000	BC	8.52	290.36	1	0.000
B^2	4.7	152.47	1	0.016	CD	−5.82	135.26	1	0.007
A^2D	−4.14	68.67	1	0.089	A^2	10.31	715.24	1	0.000
AB^2	−10.91	238.23	1	0.004	B^2	7.31	359.92	1	0.000
AC^2	−25.74	1325.02	1	0.000	D^2	5.39	195.31	1	0.002
B^2C	23.23	1438.74	1	0.000	AB^2	−7.14	101.88	1	0.016
BC^2	−9.34	232.43	1	0.004	AC^2	−26.81	1438.06	1	0.000
Residual		335.73	16		B^2C	16.12	693.05	1	0.000
Lack of fit		301.91	12	0.152	BC^2	−9.72	251.73	1	0.001
Pure error		33.81	4		Residual		191.96	14	
Cor total		8046.03	28		Lack of fit		174.64	10	0.096
R^2	0.96				Pure error		17.32	4	
Adj R^2	0.93				Cor total		7025.5	28	
Pred R^2	0.82				R^2	0.97			
Adeq precision	20.07				Adj R^2	0.94			
					Pred R^2	0.75			
					Adeq precision	22.04			